Creating and Testing Carbon Fiber Tubes

Braden Oh, Tigey Jewell-Alibhai,
Simon Kemp, Andrew Mascillaro

December 9, 2021

Table of Contents

1. Introduction

The purpose of this project was to measure the relationship between the winding angle of a carbon fiber (CF) tube and the flexural load it can support. The team's initial hypothesis was that tubes wound at lower helical angles (windings that result in tight, dense helices, rather than drawn out ones) would support greater loads than those with higher helical angles when a compressive force is applied across the tube's diameter. This investigation necessarily required the development of a system for winding CF tubes. This was achieved by building a machine capable of winding tubes in a faster, more accurate, and more repeatable manner than can be achieved by hand. With this system developed, it was used to wind two replicates of tubes at three winding angles. Research into industry methods of manufacturing CF tubes led to a manufacturing technique in which the replicate tubes were first wound out of dry filament, next painted with epoxy resin, and finally cured in a warm environment. After curing, the tubes were subjected to a compression test.

2. Methods

a. Machine Design

CF winding machines are the standard way of manufacturing tubes. These machines consist of two major components: a rotating tube (mandrel) which accepts CF filament and serves as a mold for the final tube; and a cart on a linear rail that slides back and forth along the length of the mandrel, controlling the position of the CF filament as it is wound about the mandrel. Industry machines are highly precise and very costly, so it proved a significant challenge to create a machine that can operate with reasonable precision at a fraction of the budget. An image of the assembled device is shown in Figure 0.

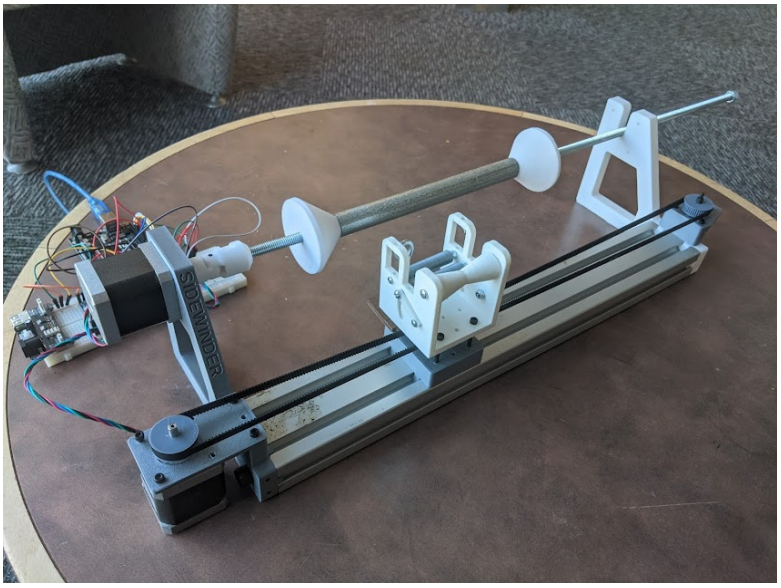

Figure 0: Sidewinder Carbon Fiber Winding Machine

The Sidewinder machine is powered by two stepper motors for high-precision control of mandrel angle and cart position. The motor controlling the cart does so via a belt to achieve translational movement. An external length of CF filament is fed through a series of rollers on the cart which tension and feed the filament onto a precise location on the rotating mandrel. The motor controlling the mandrel spins an axle directly affixed to the mandrel tube. Simultaneously rotating the mandrel and linearly moving the cart results in filament being wound in a helical pattern about the mandrel; varying the speed of the linear cart controls the helical winding angle, while varying the relative linear position of the cart and the angular position of the mandrel controls the spacing between filament strands on the final wound tube. Motor control is performed by an Arduino loaded with custom firmware. Given an inputted tube length and winding angle, custom firmware controls the motors to produce the desired winding patterns. Sidewinder also has an LCD screen with the current state of the job and a pause / resume button in case the job needs to be paused and something needs to be fixed in the middle of the winding process. All mechanical parts were 3D printed with PLA or scavenged from scraps in the machine shop. All electrical components were borrowed.

b. Tube Structure and Mandrel

Initial attempt: The initial mandrel was a brass tube 2” in diameter. The CF was wound directly on the tube then epoxied after and put into a furnace at 70℃ for 24 hours. The wind pattern consisted of 2 hoop layers and a partial helical layer. To remove the tube from the mandrel, the brass was supposed to expand in the furnace then shrink to a smaller diameter in a freezer. Thus breaking the bond between the epoxy and the brass. This proved insufficient, as the bond between the epoxy and the brass was too strong to remove the tube without breaking it.

Final design: The final iteration of the mandrel was a cardboard tube wrapped in a layer of wax paper with a layer of aluminum foil atop the wax paper. The wax paper allowed for easy removal from the mandrel tube and the foil shield was used after it was discovered that epoxy can penetrate wax paper. To prevent the fiber from slipping during the wind, there were two strips of tape spiraled around the aluminum foil surface. The CF was then wound on top of the aluminum and coated in epoxy after being removed from the machine in a process that is explained below in section c, “epoxy impregnation and cure.” The wax paper layer successfully allowed the CF and foil to be removed from the mandrel post-curing. The aluminum foil proved to be easy to remove from the epoxied CF even after curing.

The structure of the CF was chosen to maximize the quality of the tubes while varying the helical angle. The first layer was a partial helical layer at an angle of 10°, 25°, or 40°, followed by a single hoop layer on top. The partial helical was chosen because the machine was not able to consistently place the fiber adjacent to the previous pass, and the team was unable (given the time constraints on the project) to effectively tension the fiber to rolling taut without jamming the motors. This led to fears that a full helical layer would have led to a tube with an inconsistent diameter across the length, and indeed, this was still an issue with the partial helix tubes, though to a much lesser extent than with a full helix. By winding the partial helical first then by finishing the entire tube with a single hoop wind layer over the top, it was supposed that the final tube could benefit from the lateral strength of the helical layer on the bottom (and thus

helical angle could still serve as the experimental variable) and could still have a flat surface for testing, as the final hoop layer would compress the helical layer. Because this surface hoop layer was added to every replicate, it was supposed to effectively provide the identical structural support across each tube, allowing the wind angle to continue to be the variable of interest.

c. Epoxy Impregnation and Cure

There are three methods of epoxy impregnation: pre-impregnated filament (purchased commercially), wet winding (coating filament in epoxy as it is wound), and dry winding (winding the entire tube without epoxy and covering it afterwards). Due to the high cost of purchasing pre-impregnated filament, only wet and dry winds were attempted with the Sidewinder machine. The wet wind was attempted first and consisted of one team member using gloved fingers to manually coat filament in epoxy as it was wound onto the mandrel. This method ensures that all fibers receive an epoxy coating, but leads to a highly variable tension being placed on the wound filament, significantly altering the reliability of the wind pattern. Furthermore, wet filament was more difficult to have remain in place during the winding process. For these reasons the dry winding method was used for the final tubes. Each of the tested replicates were wound dry and coated in epoxy after the mandrel was removed from the machine.

The epoxy chosen for this project was West Systems 105 resin mixed with 209 “super slow” hardener. The decision to use West Systems resin was based on the toxicity requirements of the Olin composites bay. Selection of the hardener had an additional timing consideration. Hardener determines the pot life of the epoxy (the time available to apply it to a part before beginning to congeal), time to solid state, time to full strength, and working environment temperature. A dry wind does not require a long pot life so a faster hardening epoxy may be preferable to achieve full strength as quickly as possible. However, for a wet wind the pot life must be greater than the wind time of the part, meaning a slower cure is preferable. The intention of this project is to prove a system that could be used by Rocketry and DBF in the future, and despite the difficulties this team faced, a wet wind is ultimately preferable for both applications. It was thus decided that the 209 super slow hardener would be used, because it works for both wind styles. One consequence is the increased time to full strength of 4-9 days at 22° C. As curing occurs more quickly at higher environment temperatures, the sample tubes were cured in a furnace at 70° C to ensure a full cure would occur in 4 days.

One pump each of epoxy and hardener (the pumps are pre-calibrated to the correct mix ratio by West Systems) were used on each tube. Each tube was saturated in epoxy and a spoon was used to force the epoxy into the lower layers of the tube. This method was repeated until all the epoxy was applied, then the tube was wrapped in peel-ply (a fabric permeable to epoxy that epoxy will not bind to) and bleeder-breather (a fabric that absorbs epoxy). The tube was then rolled on a table so the epoxy would be more evenly distributed throughout the fiber and so that excess epoxy could be absorbed into the bleeder-breather. Finally, each tube was placed into a furnace at 70° C for 24 hours to harden to solid state. At this point the mandrel was removed by simply sliding the hardened tubes off and the tubes were placed back in the furnace for 3 days at 70° C to reach full strength prior to testing.

3. Results

In total, six CF tubes were produced: two replicates at each of three angles. The experimental helical angles were 10°, 25°, and 40°, as it was believed that these three angles could provide a representative range of behaviors across the total range of available angles, 0-45°.

a. Mass

Each of the six samples was massed and the length, inner diameter, and outer diameter were measured and used to approximate wall thickness. The samples were then tested in a diametrically applied compression test. The initial measurement data is shown in the table below:

Name	Angle	Mass (g)	Length (mm)	Wall Thickness (mm)
10-1	10° + hoop	26.89	166.00	1.25
10-2	10° + hoop	27.95	161.00	1.71
25-1	25° + hoop	33.57	170.00	1.76
25-2	25° + hoop	36.76	176.00	2.30
40-1	40° + hoop	27.36	156.00	2.43
40-2	40° + hoop	34.11	179.00	2.01

Table 0: Physical measurements of constructed tubes

The winding patterns were calculated in such a way that all samples would use the same amount of CF filament. However, the variation in masses can come from a variety of sources. One source of variation is in application of the epoxy used to bond the CF strands together. The epoxy has a non-negligible weight in the tubes because CF is so light and high variability exists in the amount of epoxy applied and squeezed out of the tubes. A second source of variation is error in the winding process. Although the rolling was controlled by the same machine, slightly different amounts of CF could have been used to create the rolls due to variabilities and unreliabilities in the filament tension and in the motor, belt, and frame configuration. A third source of variation is in the distribution of epoxy through the CF layers. Although it was supposed that saturating the tube would allow for full penetration to the bottom layers of filament, there was no effective way to measure this (one major advantage of a wet wind is that it ensures even distribution of epoxy).

b. FEA

To gain a conceptual understanding of the stresses which would be distributed throughout the body of the tubes during compression testing, FEA was performed in Solidworks to simulate the diametric compression test (see Figures 1-2).

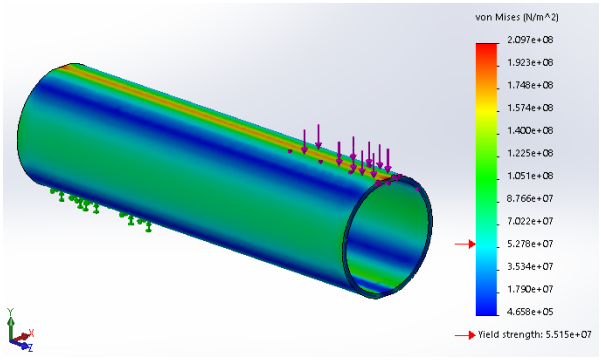

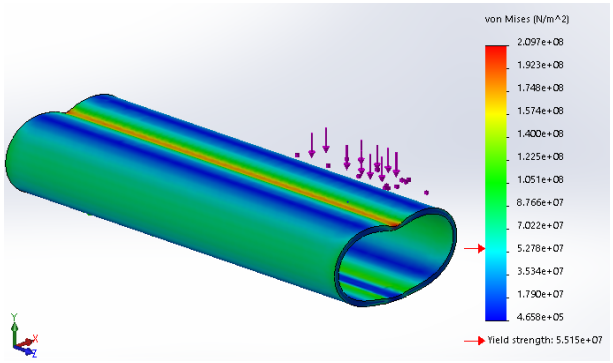

Figure 1 (left): Image showing the calculated Von Mises stress on the tube during the compression test. Note the yield strength shown is not accurate to CF, the analysis was performed on 6061 aluminum to show the location and magnitude of the stress.
Figure 2 (right): Image showing the estimated deformation of the tube after the compression test.

The FEA shows that the highest stress concentrations will be along the top and bottom of the tube as shown in Figure 1, with additional regions of high stress concentrations along each side. This is validated by the shape of the test piece after deformation. Another important thing to note is that CF is known to be strong in tension and weak in compression (graphene can withstand tensile strains of 1.3% but compressive strains of only 0.7%, see Tsoukleri, 2009), meaning the direction of the force is important when predicting failure mode.

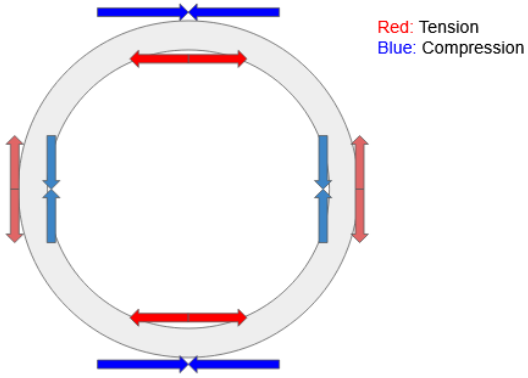

Figure 3: Directions of forces at each of the locations where stress is concentrated.

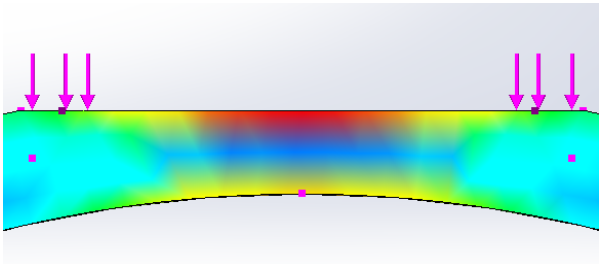

Figure 4: Close up of the Von Mises stress on top of the tube, showing the stress is higher on the outer edge (which is under compression) than the inner edge (under tension).

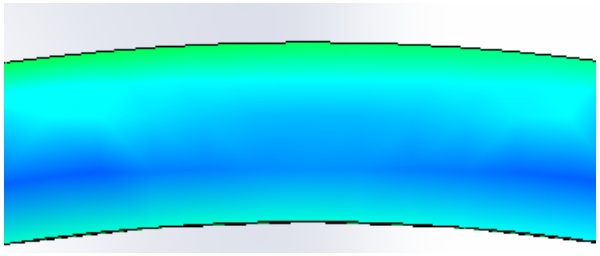

Figure 5: Close up of Von Mises stress on the side of the tube. Similar to the top, the outside (tension) has higher stress than the inside (compression).

Figures 4-5 show stress concentrations in the top and sides of the tube. From these we would expect the series of material failures to take the following order: 1. The top will cave in with the fibers on top breaking first because of high compressive force. 2. The sides would break because of lower overall stress with the majority of the force putting the fiber in tension, which is the fiber's preferred direction. Because the side walls experience greater tension forces (outside surface) than compressive forces (inside surface) it is not possible to predict whether the inner or outer fibers will break first, but it is expected that both surfaces will fail eventually in their respective manners.

c. Instron Testing

The mini-instron was outfitted with large compression test plates and the tubes were laid on their side in between the plates, so that the compressive force was applied across the diameter of the tube and nearly across its entire length, as well. A force was applied by driving the top test plate into the top of the tube tube at a constant rate of -8mm/min to a final distance of -28mm (this was beyond half of each tube's original diameter; the average tube outer diameter was 46.5mm). Stress-strain curves for these tests are shown in Figures 6 and 7 with key data points tabulated in Table 1.

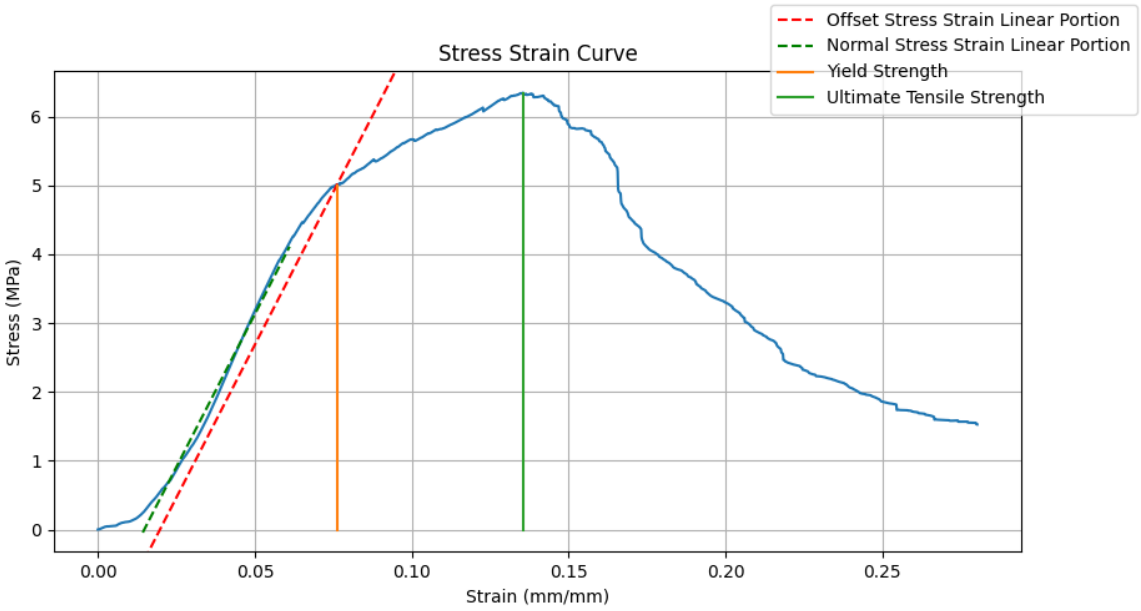

Figure 6: The stress-strain curve of the sample 10.2 load test with four primary properties marked to illustrate the graphical locations of the yield, ultimate, and linear stresses. A composite image showing the stress-strain curves of all tests is given in Figure 7, but for the sake of clarity only the ultimate tensile strength is marked in the composite image.

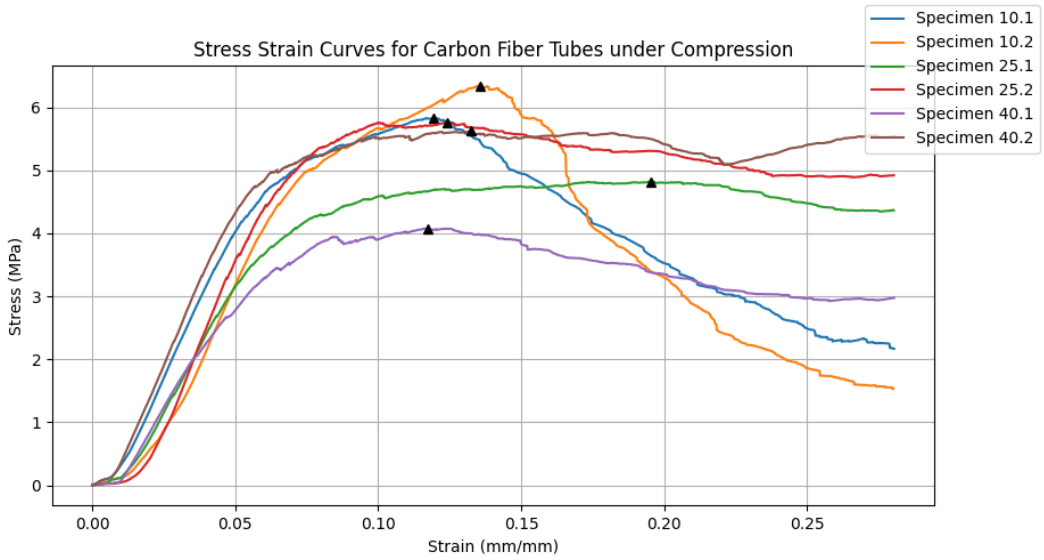

Figure 7: Composite image showing the stress-strain curves and ultimate stresses for all tested specimens. The two-number naming scheme of the specimens corresponds to the wind angle (first number) and replicate number (second number).

Sample	Modulus (MPa)	Yield Stress (MPa)	Yield Strain (mm/mm)	Ultimate Stress (MPa)
10-1	98	4.58	0.06	5.83
10-2	89	5.00	0.08	6.34
25-1	80	3.79	0.06	4.82
25-2	110	4.69	0.06	5.76
40-1	72	3.15	0.06	4.07
40-2	103	4.74	0.06	5.62

Table 1: Key individual data points for each tested sample

The data taken from these stress-strain curves was tabulated and further analyzed for correlation in Design Expert.

d. Design Expert Analysis

Design expert was used to create a single level categorical design where the wind angle was an ordinal three level factor (10°, 25°, 40°) with two replicates at each point. The uncontrolled variables mass, length, and wall thickness were included as responses in the model because of the variability in their values. The measured variables modulus, yield stress and strain, and ultimate strength were also included as responses in the model.

The correlation between wind angle and yield stress was significant with $p = 0.0348$. It is notable however, that although the error bars for 10° do not overlap with the error bars for the higher angles, the higher angles' error bars have significant overlap with each other, making the two not significantly different from one another. A graph of the one factor yield stress to wind angle correlation is shown in Figure 8. To verify that the most significant factor governing yield stress was indeed wind angle, correlations between yield stress and each of mass, length, and wall thickness were independently verified. In all three cases, there was no significant correlation, indicating that mass, length, and wall thickness likely didn't cause a false significance for yield stress.

Regarding modulus, the results were similar in that the 25° and 40° angles showed distinctly greater mean moduli than the 10° angle, but very similar means to each other. The results differed, however, in that the model was not significant, with $p = 0.1297$ and that error bar overlap occurred across all three wind angles. This is due in part to the high difference in moduli across the 25° replicates which had the effect of increasing the noise and making a signal harder to detect. A graph of the one factor modulus to wind angle comparison is shown in Figure 9.

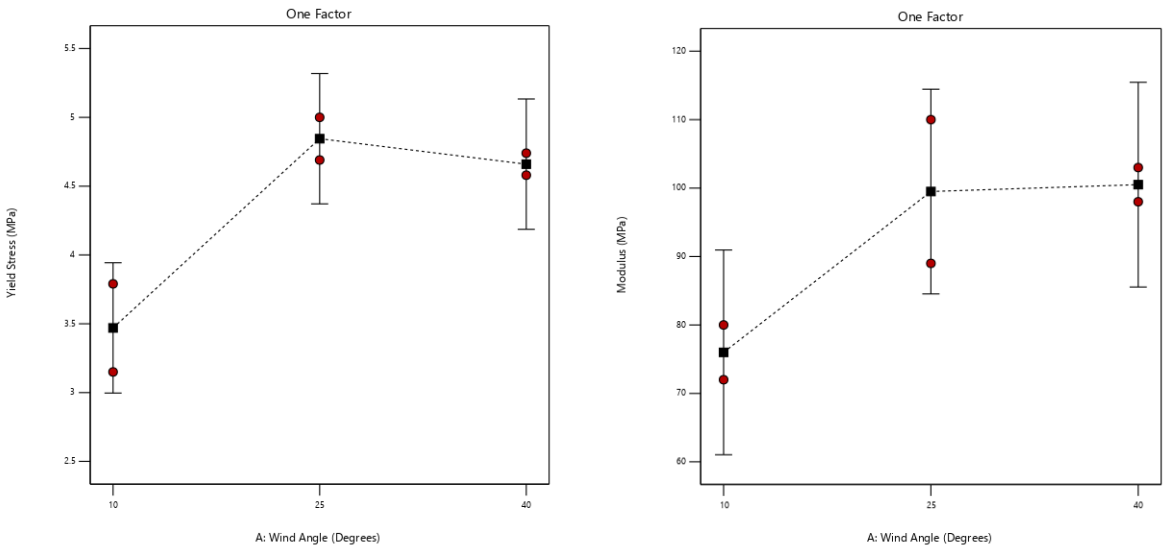

Figure 8 (left): a comparison between yield stress and wind angle. It can be noted that the yield stress is significantly correlated between the 10° samples and both higher angle samples, but the yield stresses between the 25° and 40° samples are not significantly correlated.
Figure 9 (right): a comparison between modulus and wind angle. It can be noted that the modulus is not significantly correlated to any of the three wind angles.

4. Discussion

The sample size is small at only 6 test pieces, so it is difficult to draw general conclusions from the available data. The data collected, however, does suggest that higher wind angle helical tubes outperformed the lowest angle tube on each measured metric. In other words, higher wind angle tubes appear to be stiffer and have higher yield and ultimate strengths. The 25 and 40 degree angle tube samples have similar measured properties, suggesting that diminishing returns may be reached as the angle increases above a particular threshold, but the available data is not sufficient to establish this with any significant certainty. These results contradicted our initial hypothesis that the fibers at a lower angle would be able to hold higher forces because they are supporting the load more directly. However, greater reasoning (as demonstrated below) does lead to a theory for why this outcome occurred.

a. Stress Tensor and Mohr's Circle

The new hypothesis is that compressive stresses placed on the tube are more greatly redirected to shear stresses in tubes with higher helical angles. To demonstrate this rationale, we begin with a graphical representation of the stress tensor on the side of the tube. Where $\boldsymbol{\sigma}$ is the normal stress and $\boldsymbol{\tau}$ is shear stress.

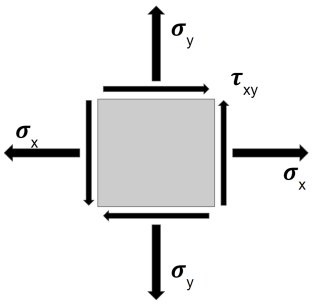

In this case the only force is a compressive force in the σ_y direction. For simplicity of the calculation we will assume σ_y is -1 and the rest of the values are zero. Because the CF strands are not parallel to the direction of the compressive stress (and ignoring the hoop layer because it is a constant across all samples) we next need to find the component stresses at the angle of the helical.

To find the stress at a given angle the following stress transformation equations related to Mohr's Circle can be used:

$$\sigma_{x'} = \frac{\sigma_x+\sigma_y}{2} + \frac{\sigma_x-\sigma_y}{2}cos(2\theta) + \tau_{xy}sin(2\theta)$$

$$\sigma_{y'} = \frac{\sigma_x+\sigma_y}{2} - \frac{\sigma_x-\sigma_y}{2}cos(2\theta) - \tau_{xy}sin(2\theta)$$

$$\tau_{x'y'} = -\frac{\sigma_x-\sigma_y}{2}sin(2\theta) + \tau_{xy}cos(2\theta)$$

Using a value of -1 for compressive stress in the Y direction yields the following table of stress values at each tested wind angle:

Angle	σ_x - Normal stress x	σ_y - Normal stress y	τ_{xy} - Shear stress
10	-0.0302	-0.970	-0.171
25	-0.179	-0.821	-0.383
40	-0.413	-0.587	-0.492

Table 2: Forms of stress based on the stress transformation equations for each angle, showing the increasing shear stress as the angle increases.

This shows numerically that as angle increases the stress translated to shear increases as well. This is visible as well in Mohr's circle as shown to the right. As the angle of the wind increases, the shear also increases until a 45° angle is reached, at which point shear begins to decrease again. Another thing to note is that the normal stress is always negative; this correlates to compressive stress. If the CF composite behaves stronger in shear stress than in compression (the aforementioned paper Tsoukleri, 2009 only provides data on graphene in tension, not in shear), then the

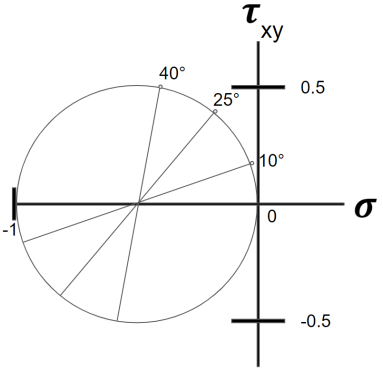

40° and 25° helical angles would expectedly perform significantly better than the 10° angle, with only a small difference between the 40° and 25°. This is exactly the outcome observed in the test data.

The “if” in the new hypothesis is whether the CF composite material behaves strongly under shear loading. Mohr’s circle is applied to a square element of the composite material, so the macrostructure of the composite CF/epoxy fiber structure needs to be considered. Because helical winding occurs both forwards and backwards, the CF fibers effectively form an X shape (low wind angles would see highly vertical, narrow X’s, while high wind angles would see wide X’s, see Figures 10 and 11). Shear loading on this macrostructure is necessarily resisted by the fibers. Consider the simple cases of 0° and 45° winding. In 0° winding (similar to a hoop layer, see Figure 10) the CF strands are all parallel to one another, so the applied load can only be experienced as an in-line compressive stress. In 45° winding (see Figure 11), some of the applied load is converted into shear stress, parallel to the cross-woven fibers. This has the effect of placing each set of fibers under tension and reduces the in-line normal loading. In effect, wind angles execute a stress transformation on the elements of the CF composite material, translating some of the applied load on the tube into tensile strains on the CF fibers. This enhances the entire material’s performance under the overall diametric compressive load.

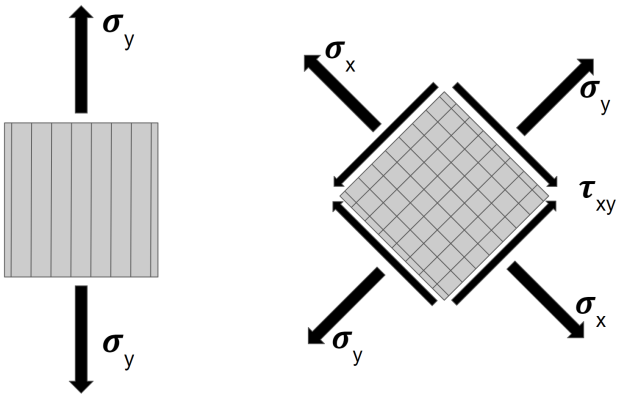

Figure 10 (left): for a low wind angle element (example 0°) the only applied forces are negative normal forces, parallel to the vertical set of CF fibers which are prone to buckling under compressive stress.
Figure 11 (right): for a high wind angle element (example 45°) some of the overall applied normal force is translated into shear stress which places the CF fibers into tension. This has the effect of reducing the normal loading (parallel to the direction of the fibers) on the CF composite element.

This implies two failure modes for the material: either the applied shear load breaks the epoxy matrix holding parallel CF fibers together, or the compressive force applies such a strong normal force to a CF element that the fibers buckle under compression.

b. Future work

The immediate next step is to validate this new hypothesis. This validation could be performed by using the same Sidewinder tube production setup to produce more replicates and to do so at a higher number of angles to prove whether the relationship implied by Mohr's circle truly exists. If this hypothesis can be validated then sufficient understanding of the mechanisms behind force loading in CF composite macrostructures is known to allow larger tubes to be produced for the DBF and Rocketry teams. This will, in turn, necessitate a larger and more precise tube winder.

c. Conclusion

The purpose of this project was to measure the relationship between the winding angle of a CF tube and the flexural load it can support. The team's initial hypothesis, that tubes wound at lower helical angles would support greater loads than those with higher helical angles, was disproven given the collected data. The collected data, while not representative enough to prove a highly certain relation, suggests that the opposite is true: higher angles support greater loads. It is believed that this is due to higher wind angles resulting in greater translation of compressive to shear forces in the composite material, translating into greater tensile and lower in-line loading on the CF filaments. Future investigation with a greater variety of wind angles and number of replicates should be performed to verify this new hypothesis prior to the application of CF tubes for critical DBF and Rocketry components.